Supporting Information

Weaving microscale wool ball-like hollow covalent organic polymers from nanorods for efficient adsorption and sensing

Guihan Cai[a], Tongtao Wang[a], Qisheng Wei[b], Chaoying Tong[a], Yuanxin Cao[b], Shuyun Shi[a,b,c]*, Yuxia Chen[a], Ying Guo[c]*

[a]College of Chemistry and Chemical Engineering, Central South University, Changsha 410083, Hunan, China

[b]Natural Product Research Laboratory, Guangxi Baise High-tech Development Zone, Baise 533612, Guangxi, China

[c]Department of Clinical Pharmacology, Xiangya Hospital, Hunan Key Laboratory of Pharmacogenetics, Central South University, Changsha 410078, Hunan, China

*Corresponding authors: Tel./fax: +86 731 88879616.

E-mail addresses: shuyshi@csu.edu.com (S. Shi), guoying881212@csu.edu.cn (Y. Guo).

1. Experimental section

1.1. Materials and apparatus

Bisphenol A (BPA, 99 %), 3,3',5,5'-tetrabromobisphenol A (TBBPA, 98 %), sulfamethoxazole (SMZ, 99 %), 1,3,5-triformylphloroglucinol (TP, 97 %), and 3,3',5,5'-tetramethylbenzidine (TMB, 98 %), were supplied by Aladdin Biochemical Pharmaceutical Co., Ltd (Shanghai, China). Hydrochloric acid (HCl), sodium hydroxide (NaOH), cetyltrimethyl ammonium, triton X-100, sodium laurylsulfonate, dioxane, mesitylene, glacial acetic acid (≥ 99.7 %), methanol, acetonitrile, *N*-methylpyrrolidone, tetrahydrofuran, anhydrous ethanol, *N*,*N*-dimethylacetamide, *N*,*N*-dimethylformamide, Li_2SO_4, NaCl, KCl, $AgNO_3$, $BaCl_2$, $Ni(NO_3)_2$, $CuCl_2$, $MgSO_4$, $CaCl_2$, $FeCl_2$, $Cd(NO_3)_2$, $CoCl_2$, $MnCl_2$, $AlCl_3$, and $CrCl_3$ were acquired from Sinopharm Chemical Reagent Co., Ltd (Shanghai, China). HPLC grade methanol and formic acid were obtained from Sigma-Aldrich Trading Co. Ltd (Shanghai, China). Ultrapure water was generated in Milli-Q water system (Millipore, Bedford, MA, USA) and used in all experiments.

Fourier transform infrared (FT-IR) spectra were collected on a Nicolet 6700 FT-IR spectrometer (Thermo, MA, USA) with the recorded wavenumbers from 400 to 4000 cm^{-1}. Powder X-ray diffraction (PXRD) data were tested by a MiniFlex600 Powder X-ray diffractometer (Rigaku, Japan) at 15 mA and 40 kV using Cu Kα radiation (scan speed: 10 deg/min). The N_2 adsorption and desorption isotherms data of materials were collected on a Kubo X1000 pore and surface area analyzer at 77 K (Biaode, Beijing, China). The synthesized materials were outgassed at 180 °C for 8 h to 12 h. The surface areas were calculated by Brunauer-Emmett-Teller (BET) methods, and the pore-size-distribution data were obtained through the non-local density functional theory (NLDFT). Thermogravimetric analysis (TGA) for materials was

carried out on a TGA2 thermal gravimetric analyzer (Mattler Toledo, Switzerland) in the N_2 atmosphere (20 mL min^{-1}), and the temperature was tested from room temperature to 800 °C with a constant heating rate of 10 °C min^{-1}. Water contact angle was carried out on the instrument (JC2000D1, Powereach Co. Ltd, Shanghai, China). Fluorescence spectra were collected on a F-9000 spectrofluorometer (Hitachi, Japan) with the scan speed at 1000 nm min^{-1} and the photomultiplier tube voltage of 700 V. Fluorescent decay time curves for MWH-COPs (0.02 mg mL, aqueous solution) before and after addition of BPA (1.0 mg L^{-1}) were collected at room temperature on a Fluo Time 100 spectrofluorometer (PicoQuant, Germany) using excitation at 365 nm and emission at 578 nm. The fluorescent lifetime was calculated using the average lifetime model. The Zeta potential of COPs nanorods and particle size of emulsion were monitored on Malvern Zetasizer Nano ZS (Malvern, UK). Morphology of materials was characterized with a JSM-7900F scanning electron microscopy (SEM, JEOL, Japan), which operated at 5 kV, and a Tecnai G2 20S-Twin transmission electron microscope (TEM, FEI, Prague, Czech). High performance liquid chromatography (HPLC) with Zorbax SB-C_{18} column (150 mm × 4.6 mm i.d., 5 μm) and UV detector at 276 nm was used for analysis (Agilent Technologies, Santa Clara, CA). HPLC-grade methanol and aqueous solution of 0.1 % formic acid (7/3, *v*/*v*) was applied as mobile phase with a flow rate at 0.8 mL min^{-1}.

1.2. Synthesis of COPs nanorods, MWH-COPs and B-COPs

COPs nanorods were firstly synthesized by an emulsion polymerization method. Briefly, TP (42 mg, 0.2 mmol) or TMB (72 mg, 0.3 mmol) was dissolved in mesitylene (6 mL) to form a transparent oil phase solution. Then the oil phase solution was added into the aqueous phase containing water (12 mL) and triton X-100 (0.2 mL). After vigorous stirring at 500 rpm for 5 min, two immiscible phases were emulsified into a

stable white emulsion. Subsequently, the emulsion of TP was slowly dripped into the emulsion of TMB at room temperature and magnetically stirred at 500 rpm for 1 h for Schiff-base reaction. Finally, yellow COPs nanorods were obtained by centrifuge at 10000 rpm for 15 min and washed with dioxane–mesitylene solution (1:1, *v*/*v*, 10 mL) 3 times. Obtained COPs nanorods were then dispersed in dioxane–mesitylene solution (1:1, *v*/*v*, 6 mL) and acetic acid solution (0.5 mL, 6 mol L^{-1}) in a dry Schlenk storage tube (25 mL), which was left undisturbed at 120 °C for 3 days. Solid products were washed with anhydrous ethanol (6mL, 3 times) and *N*,*N*-dimethylformamide (DMF) (6mL, 3 times), and then extracted by a Soxhlet extractor with anhydrous THF (100 mL) for 24 h to completely remove impurities. MWH-COPs (89.0 mg, 78.1 % yield) was finally achieved after being dried at 60 °C for 24 h under vacuum oven.

By comparison, B-COPs was directly synthesized by solvothermal method as follows. TP (42 mg, 0.2 mmol) and TMB (72 mg, 0.3 mmol) were added into dioxane–mesitylene solution (1:1, *v*/*v*, 6 mL) and acetic acid solution (0.5 mL, 6 mol L^{-1}) in a dry Schlenk storage tube (25 mL). After degassing by a three freeze-pump-thaw cycle system, the Schiff-base reaction was conducted at 120 °C for 3 days. Solid products were washed, Soxhlet extracted, and dried as those described for MWH-COPs to give B-COPs (102.6 mg, 90.0 % yield).

1.3. Adsorption kinetics studies

Adsorption kinetic experiments were conducted as follows. B-COPs or MWH-COPs (10.0 mg) was mixed with BPA aqueous solution (100 mL, 50.0 mg L^{-1}). After shaking at a thermostatic oscillator at 298 K, samples (2 mL) were withdrawn at designated time intervals (10, 15, 20, 25, 30, 50, 80, 120, 180, 300 min for B-COPs, and 1, 2, 3, 4, 5, 6, 8, 10, 15, 30, 60 min for MWH-COPs), filtered by 0.22 μm membrane, and subjected to high performance liquid chromatography (HPLC) analysis.

BPA concentrations at different times (C_t, mg L^{-1}) were obtained, from which the adsorption capacities at different time intervals (q_t, mg g^{-1}) could be calculated as:

$$q_t = (C_0 - C_t) * V)/m \quad (1)$$

where C_0 (mg L^{-1}) is the BPA concentration of initial solution, V (L) was the volume of solution and m (g) was the amount of B-COPs or MWH-COPs.

Three conventional kinetic models (pseudo-first-order, pseudo-second-order, and intraparticle diffusion models) were applied to fit the adsorption kinetic data and employed to investigate the adsorption process of BPA onto B-COPs or MWH-COPs. Three kinetic models were described as follows.

The pseudo-first-order model: $$\ln (q_e - q_t) = -k_1 * t + \ln q_e \quad (2)$$

The pseudo-second-order model: $$t/q_t = t/q_e + 1/(k_2 * q_e^{\,2}) \quad (3)$$

The intraparticle diffusion model: $$q_t = k_P * t^{1/2} + C_i \quad (4)$$

Herein, q_e (mg g^{-1}) is the BPA equilibrium adsorption capacity, q_t (mg g^{-1}) is the adsorption capacity at different time intervals, k_1 (min^{-1}) and k_2 [g mg^{-1} min^{-1})] are the rate constant of the pseudo-first-order and pseudo-second-order kinetics model; k_p (mg g^{-1} $min^{-1/2}$) represents the diffusion rate constant of BPA, C_i (mg g^{-1}) is a constant related to the thickness of the boundary layer of B-COPs or MWH-COPs.

1.4. Adsorption isotherm analysis

To construct the BPA adsorption equilibrium experiments, B-COPs or MWH-COPs (10.0 mg) was mixed with BPA solution (100 mL) with various concentrations (C_0, 10, 20, 30, 40, 50, 70, 90, 120, 150, 200 mg L^{-1}) at three different temperatures (298 K, 308 K, 318 K). After shaking the series of solutions at a thermostatic oscillator at 298 K for 15 min, solutions were filtered by 0.22 μm membrane and subjected to HPLC analysis. The equilibrium adsorption capacity q_e (mg g^{-1}) was calculated as

follows:

$$q_e = (C_0 - C_e) * V)/m \quad (5)$$

where C_e (mg L^{-1}) is the BPA concentration after adsorption equilibrium.

The Langmuir and Freundlich isotherm models were applied to fit the adsorption results of BPA, and further to explore the adsorption process and assess the surface adsorption performances of BPA onto MWH-COPs. Equations (4) and (5) were used to describe the Langmuir and Freundlich isotherm models.

$$q_e = (q_m * k_L * C_e)/(1 + k_L * C_e) \quad (6)$$

$$q_e = k_F * (C)\text{^}(^1/_n) \quad (7)$$

Herein, C_e (mg L^{-1}) is the BPA concentration after adsorption equilibrium, q_m (mg g^{-1}) is the theoretical isotherm saturation adsorption capacity of MWH-COPs, k_L (L mg^{-1}) is the Langmuir isotherm constant, relating to the affinity of the binding sites, k_F [(mg g^{-1}) (mg $L^{-1})^{-1/n}$] is the Freundlich affinity constant related to adsorption capacity, and n is the exponential coefficient and referred the adsorption intensity. n is the heterogeneity factor related to the adsorption intensity of the adsorbent, n>1 is for the preferential adsorption, and n<1 indicates that the adsorption is multi-layer adsorption.

Three thermodynamics parameters including the standard Gibbs free energy (ΔG^0), standard entropy change (ΔS^0) and standard enthalpy change (ΔH^0) were calculated to investigate the effect of temperature. Standard Gibbs free energy change ΔG^0 (kJ/mol) was calculated using equation (6).

$$\Delta G^0 = - RT\ lnK_c \quad (8)$$

where R (J mol^{-1} K^{-1}) represents the ideal gas constant and T (K) was the absolute temperature. K_c (L g^{-1}) represents the thermodynamic equilibrium constant, which

could be calculated by equation (7):

$$K_c = q_e/C_e \quad (9)$$

Standard enthalpy change (ΔH^0, kJ mol^{-1}) and standard entropy change (ΔS^0, J mol^{-1} K^{-1}) could be calculated by equation (8):

$$\ln K_c = \Delta S^0/R - \Delta H^0/RT \quad (10)$$

1.5. Fluorescence sensing of BPA

MWH-COPs (2.0 mg) was added into deionized water (10 mL) and ultrasonicated to prepare a steady suspension. Then MWH-COPs aqueous solution (200 μL) was mixed with BPA aqueous solution (1.8 mL) with different concentrations (0–1.2 mg L^{-1}), which was incubation at 298 K for 15 min. The fluorescent spectra were achieved with excitation wavelength at 365 nm and emission wavelengths from 450 nm to 700 nm. For investigating the practicability, the interference of some common metal ions and structural analogues (3,3',5,5'-tetrabromobisphenol A, TBBPA; sulfamethoxazole, SMZ) with concentrations at 50 mg L^{-1} was investigated. Real water samples (tap water and drinking water) spiked with four different concentrations (0.060, 0.200, 0.500, and 0.800 mg L^{-1}) were also evaluated. The limit of detection (LOD) was calculated according to the $3\sigma/k$ principle, where σ represents the standard deviation of 10 times blank measurements and k means the slope of the calibration curve.

1.6. Computational studies

Density functional calculations (DFT) were selected to elucidate the adsorption of BPA onto WHM-COPs. Dmol3 package in Materials Studio 2019 were used. An atom-centered grid was used for the atomic basis function. The dual numerical polarization (DNP4.4) all-electron basis set was selected as the electronic basis set. The self-consistent field convergence value was 1.0×10^{-6}. The conductor-like screening model (COSMO) with a permittivity of 78.54 (water) was used to mimic structures encased

by the aqueous layer. A simple structure unit was selected as the model of WHM-COPs. The adsorption binding energy is the difference between the energy of the BPA–WHM-COPs complex and the energy of the isolated BPA and WHM-COPs.

Table S1 Constants of the kinetic data for the adsorption of BPA on MWH-COPs according to the first-order-rate and the pseudo-second-order rate equation.

	Pseudo-first-order			Pseudo-second-order		
$q_{e,exp}$ (mg g^{-1})	$q_{e,c}$ (mg g^{-1})	k_1 (min^{-1})	R^2	$q_{e,c}$ (mg g^{-1})	$k_2 \times 10^{-4}$ (g mg^{-1} min^{-1})	R^2
258.64	99.58	0.13	0.902	268.10	23.30	0.997

Table S2 Constants of the kinetic data for the adsorption of BPA on MWH-COPs, and B-COPs according to intraparticle diffusion model.

	Initial Phase			Secondary Phase			Tertiary Phase		
	k_{p1} (mg g^{-1} $min^{-1/2}$)	C_1 (mg g^{-1})	R^2	k_{p2} (mg g^{-1} $min^{-1/2}$)	C_2 (mg g^{-1})	R^2	k_{p3} (mg g^{-1} $min^{-1/2}$)	C_3 (mg g^{-1})	R^2
MWH-COPs	146.333	–87.491	0.976	25.948	161.846	0.987	0.697	253.245	0.998
B-COPs	16.926	10.956	0.996	7.704.	57.658	0.999	0.162	134.671	0.994

Table S3. Maximum adsorption capacity for BPA exhibited by reported adsorbents.

Adsorbent[a]	Experimental conditions	Adsorption time (min)	q_m (mg/g)	Ref.
Fe_3O_4@TpND	T = 298 K, pH = 6.0	60	114.97	1
γ-CDP	T = 298 K, pH = 7.0	10	122.76	2
BMDCs	T = 298 K, pH = 7.0	720	714.00	3
CD/CA-*g*-PDMAEMA	T = 298 K, pH = 6.5	1440	79.00	4
MAP-GBM	T = 293 K, pH = 7.0	2880	324.00	5
BC_{MW}-*β*-CD	T = 293 K, pH = 5.5	15	209.20	6
β-Cyclodextrin/ZrO_2	T = 293 K, pH = 5.5	180	174.90	7
COF-based monolith	T = 293 K, pH = 7.0	3	61.30	8
MWH-COPs	T = 298 K, pH = 7.0	15	358.15	This work

[a]Fe_3O_4@TpND: magnetic covalent organic frameworks synthesized by 1,3,5-triformylphoroglucinol and 1,5-naphalenediamine; *γ*-CDP: *γ*-cyclodextrin polymer; BMDCs: Zn_8(adenine)$_4$(biphenyldicarboxylate)$_6$O-derived carbons; CD/CA-g-PDMAEMA: citric acid cross-linked β-cyclodextrin polymer modified with 2-dimethylamino ethyl methacrylate monomer (PDMAEMA); MAP-GBM: graphene-based monolithsynthesized by chemical reduction of Graphene oxide using magnesium ascorbyl phosphate; BC_{MW}-*β*-CD: *β*-cyclodextrin functionalized rice husk-derived biochar synthesized via microwave; *β*-CD/ZrO_2: *β*-cyclodextrin/ZrO_2 nanocomposite.

Table S4 Correlative parameters for the adsorption of BPA on MWH-COPs according to the Langmuir and Freundlich models.

	Langmuir isotherm			Freundlich isotherm		
T (K)	q_m (mg g^{-1})	k_L (L mg^{-1})	R^2	$1/n$	k_F [(mg g^{-1}) (mg L^{-1}) $^{-1/n}$]	R^2
298	379.397	0.103	0.985	0.344	74.074	0.956

Table S5 Adsorption thermodynamic parameters for the adsorption of BPA on MWH-COPs at 298 K, 308 K and 318 K.

T (K)	lnK_c	ΔG^0 (kJ mol^{-1})	ΔH^0 (kJ mol^{-1})	ΔS^0 (J mol^{-1} K^{-1})
298	4.397	–10.895		
308	4.077	–10.440	–22.888	–40.315
318	3.817	–10.091		

Table S6 Spiked recovery results for the determination of BPA in water samples.

	Added ($mg\ L^{-1}$)	Determined ($n = 3$, $mg\ L^{-1}$)	Recovery (%)	RSD (%)
Tap water	0	/	/	/
	0.060	0.063	104.75	8.08
	0.200	0.189	94.34	7.23
	0.500	0.499	99.80	5.83
	0.800	0.819	102.28	6.09
Drinking water	0	/	/	/
	0.060	0.056	93.33	5.78
	0.200	0.196	97.80	9.55
	0.500	0.488	97.65	8.05
	0.800	0.833	104.30	6.26

Table S7 Comparison of the proposed fluorescence sensing method with some fluorescence sensing methods for BPA detection.

Materials[a]	adsorption	LODs (μg L^{-1})	Ref.
M-R-MIP@d-NPs	NO	6.6	9
GBIN@NC	NO	1.8	10
FeO_x/ZnS@MIPs	YES (50.92 mg g^{-1})	0.36	11
MIP@Uio-66-NH_2@paper	YES (120.94 mg g^{-1})	0.16	12
Cr_2O_3@MIPs	NO	3.4	13
Ga-MOF	NO	6.0	14
MWH-COPs	YES (358.15 mg g^{-1})	8.0	This work

[a]M-R-MIP@d-NPs : Ratiometric fluorescence molecularly imprinted sensor based on carbon dots and gold nanoclusters; GBIN@NC: Graphene quantum dots immobilized on molecularly imprinted nanoparticles which were placed on nitrocellulose paper; FeO_x/ZnS@MIPs: Molecularly imprinted polymers on FeO_x and ZnS quantum dot nanoparticles; MIP@Uio-66-NH_2@paper: A paper-based analytical device was prepared using a metal-organic framework of UiO-66NH_2 coated with molecularly imprinted polymers; Cr_2O_3@MIPs: Molecularly imprinted polymer shell on chromium (III) oxide nanoparticles; Ga-MOF: MOF based on Ga(III) ion

References

1 D. Wei, J. Li, Z. Chen, L. Liang, J. Ma, M. Wei, Y. Ai and X. Wang, *J. Mol. Liq.*, 2020, **301**, 112431.

2 P. Tang, Q. Sun, Z. Suo, L. Zhao, H. Yang, X. Xiong, H. Pu, N. Gan and H. Li, *Chem. Eng. J.,* 2018, **344**, 514–523.

3 B. N. Bhadra, J. K. Lee, C.-W. Cho and S. H. Jhung, *Chem. Eng. J.,* 2018, **343**, 225–234.

4 Y. Zhou, Y. Hu, W. Huang, G. Cheng, C. Cui and J. Lu, *Chem. Eng. J.,* 2018, **341**, 47–57.

5 Z. Fang, Y. Hu, X. Wu, Y. Qin, J. Cheng, Y. Chen, P. Tan and H. Li, *Chem. Eng. J.,* 2018, **334**, 948–956.

6 J. Qu, M. Dong, S. Wei, Q. Meng, L. Hu, Q. Hu, L. Wang, W. Han and Y. Zhang, *Carbohydr. Polym.*, 2020, **250**, 117003.

7 M. Usman, A. Ahmed, Z. Ji, B. Yu, Y. Shen and H. Cong, *Sci. Total. Environ.*, 2021, **784**, 147207.

8 Z. Liu, H. Wang, J. Ou, L. Chen and M. Ye, *J. Hazard. Mater.*, 2018, **355**, 145–153.

9 H. Lu and S. Xu, *Biosens. Bioelectron.*, 2017, **92**, 147–153.

10 R. Uzek, E. Sari, S. Senel, A. Denizli and A. Merkoci, *Microchim. Acta.*, 2019, **186**, 218.

11 X. Zhang, S. Yang, W. Chen, Y. Li, Y. Wei and A. Luo, *Polymers*, 2019, **11**, 1210.

12 L. Zeng, X. Zhang, X. Wang, D. Cheng, R. Li, B. Han, M. Wu, Z. Zhuang, A. Ren, Y. Zhou and T. Jing, *Biosens. Bioelectron.*, 2021, **180**, 113106.

13 M. Saraji and S. Alijani, *Spectrochim. Acta A*, 2021, **255**, 119711.

14 H. Yang, B. Wang, J.H. Liu, J. Cheng, L. Yu, J. Yu, P. Wang, J.R. Li and X. Su, *Sensor. Actuator. B*, 2020, **314**, 128048.

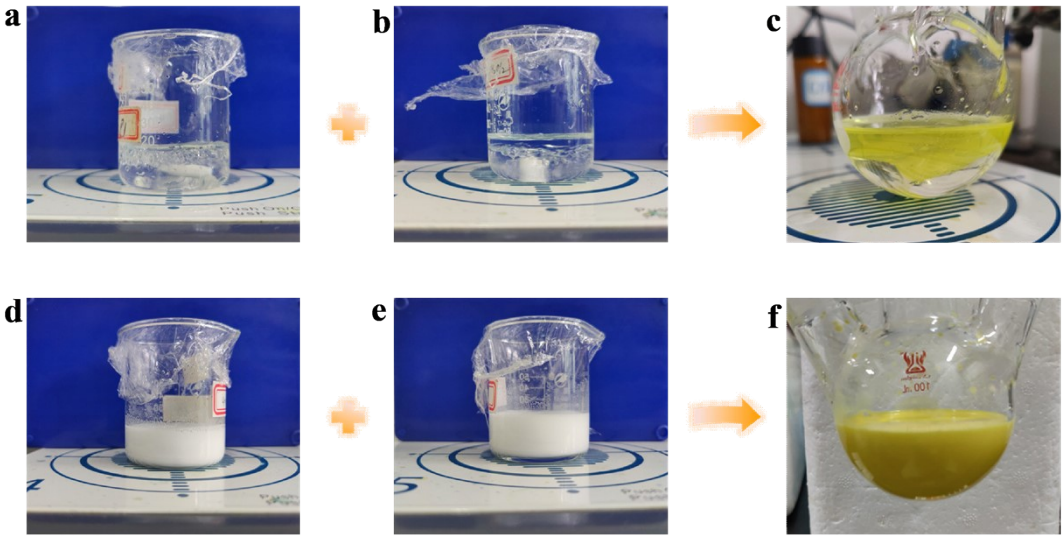

Fig. S1. Optical images of TP (a), TMB (b), and TP+TMB (c) in mesitylene–water (1:2, *v*/*v*) solution; Photograph of TP (d), TMB (e), and TP+TMB (f) in mesitylene–water (1:2, *v*/*v*) solution with triton X-100.

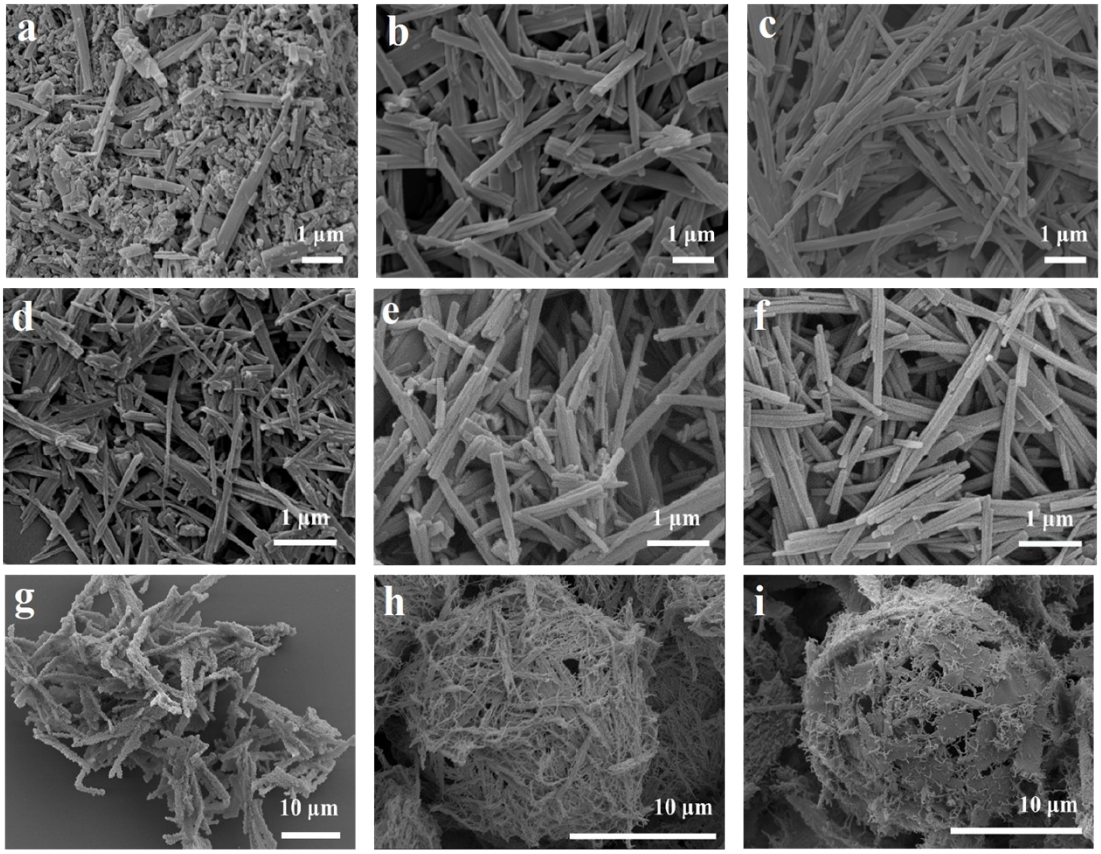

Fig. S2. SEM images of COPs nanorods by adding TP (21 mg, a; 42 mg, b; 63 mg, c) and TMB (72 mg). SEM images of COPs nanorods synthesized at 20 min, 18.6 % yield (d); 40 min, 72.2 % yield (e); 60 min, 92.6 % yield (f). SEM images of MWH-COPs by adding aqueous acetic acid at 3 mol L^{-1} (g), 6 mol L^{-1} (h), and 9 mol L^{-1} (i).

When the amount of TP was 42 mg, dispersed and uniform COPs nanorods were synthesized (Fig. S2a–2c); Length and diameter of COPs nanorods enlarged with the increasement of reaction time, and COPs nanorods with relatively uniform length and diameter were formed (length at about 3 μm and diameter at 100–200 nm) when the reaction time was at 60 min (Fig. S2d–2f). The highest yield (92.6 %) was achieved with reaction time at 60 min; COPs nanorods wove to unique and stable wool ball-like hollow microspheres (diameter at about 15 μm) when the concentration of aqueous acetic acid was 6 mol L^{-1} (Fig S2g–i).

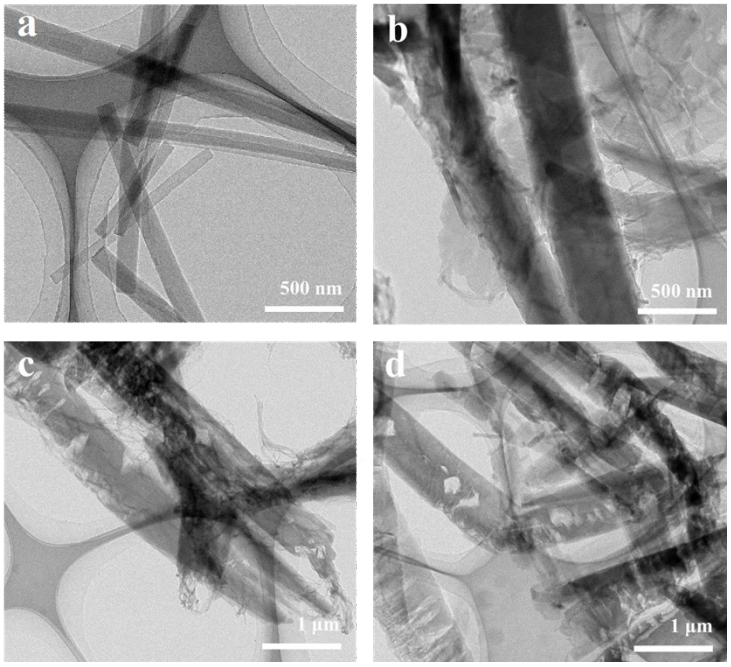

Fig. S3. TEM images of COPs nanorods (a) and MWH-COPs synthesized for 1 day (b), 2 days (c), and 3 days (d). The dissolution of COPs nanorods and recondensation of them can be observed, and the COPs nanorods are solid.

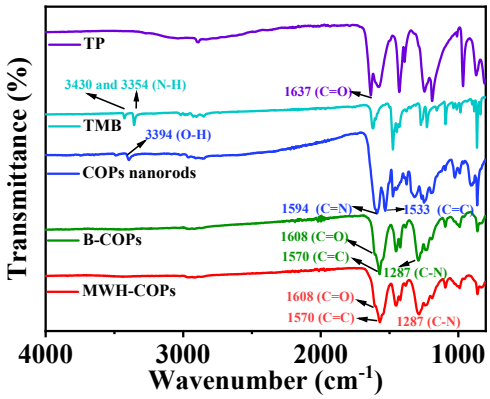

Fig. S4. FT-IR spectra of TP, TMB, COPs nanorods, MWH-COPs, and B-COPs.

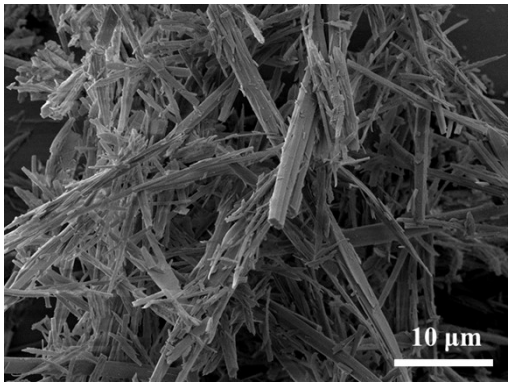

Fig. S5. SEM image of COPs rods synthesized in mesitylene–water (1:2, *v*/v) solution.

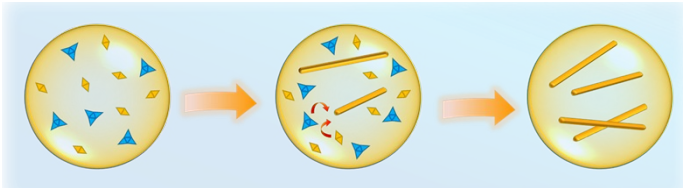

Fig. S6. Schematic diagram for emulsion-mediated formation of COPs nanorods.

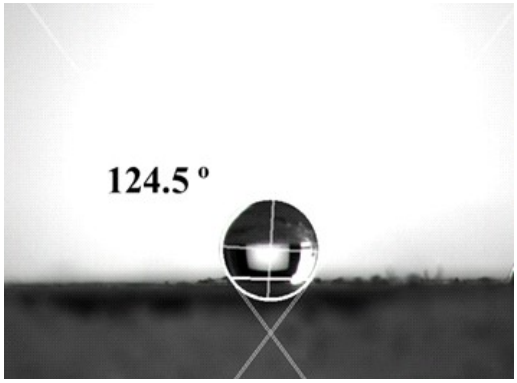

Fig. S7. Photographs of water on the surface of COPs nanorods.

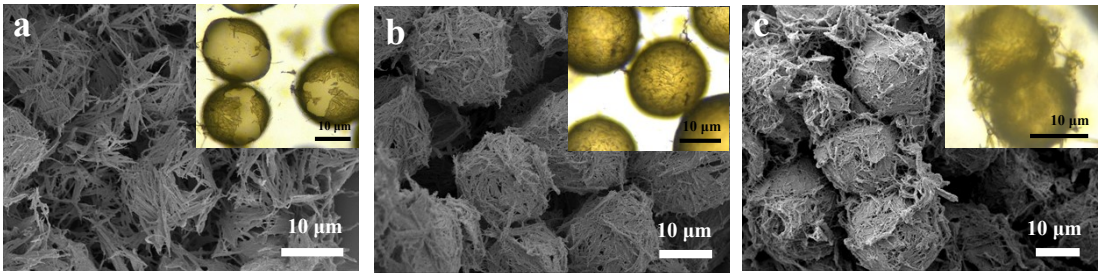

Fig. S8. SEM images of MWH-COPs synthesized by adding different amounts of COPs nanorods at 30 mg (a), 90 mg (b), and 150 mg (c) (insets were the optical microscopes of Pickering emulsion).

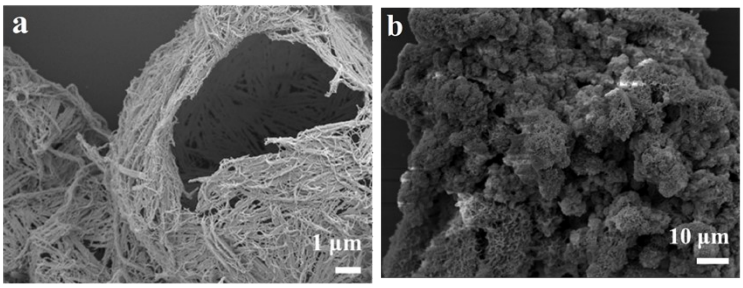

Fig. S9. SEM images of partially broken MWH-COPs (a) and B-COPs (b).

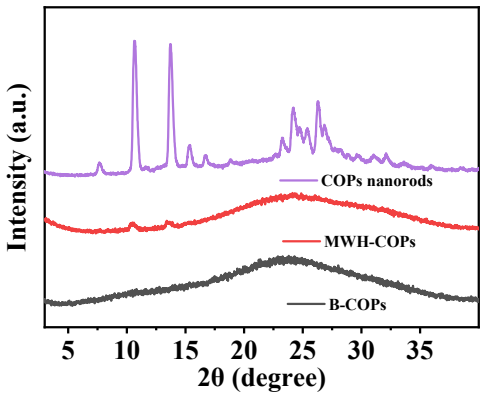

Fig. S10. PXRD patterns of COPs nanorods, MWH-COPs, and B-COPs.

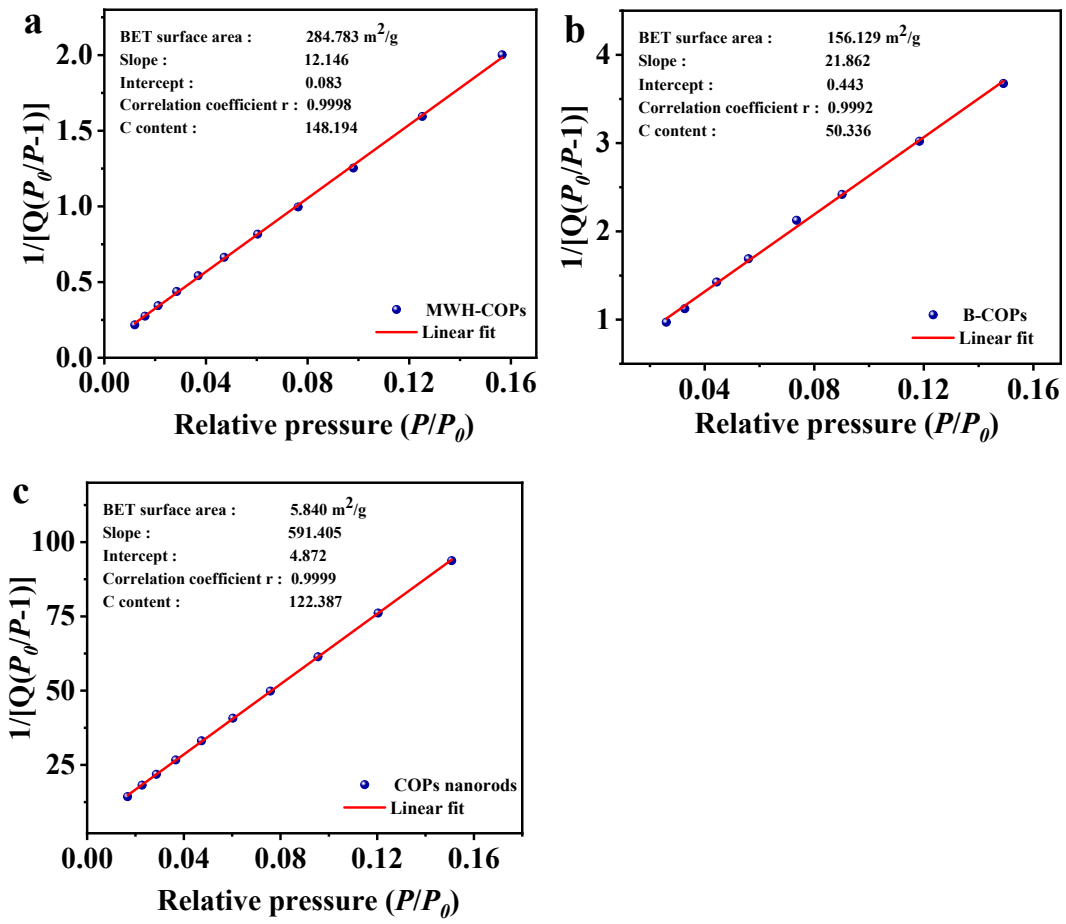

Fig. S11. Multi-Point BET fit of MWH-COPs (a), B-COPs (b), and COPs nanorods (c) obtained using adsorption isotherms at 77 K.

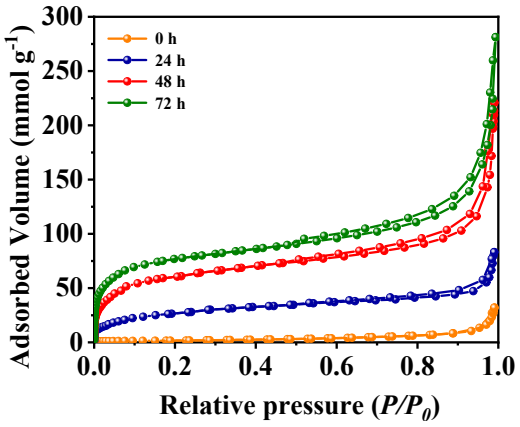

Fig. S12. Time dependent N_2 sorption isotherms of the formation of MWH-COPs.

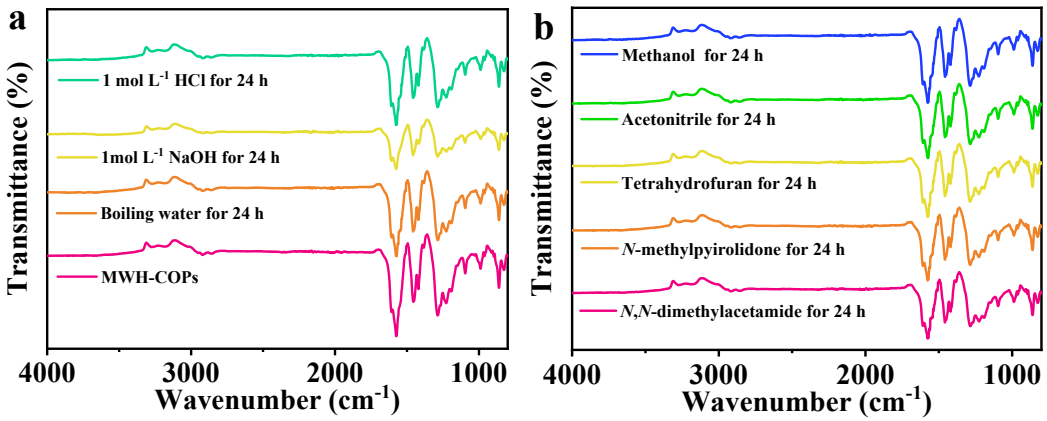

Fig. S13. FT-IR spectra of MWH-COPs after being immersed in boiling water, 1 mol L^{-1} NaOH, 1 mol L^{-1} HCl, methanol, acetonitrile, tetrahydrofuran, *N*-methylpyrrolidone, and *N*,*N*-dimethylacetamide for 24 h.

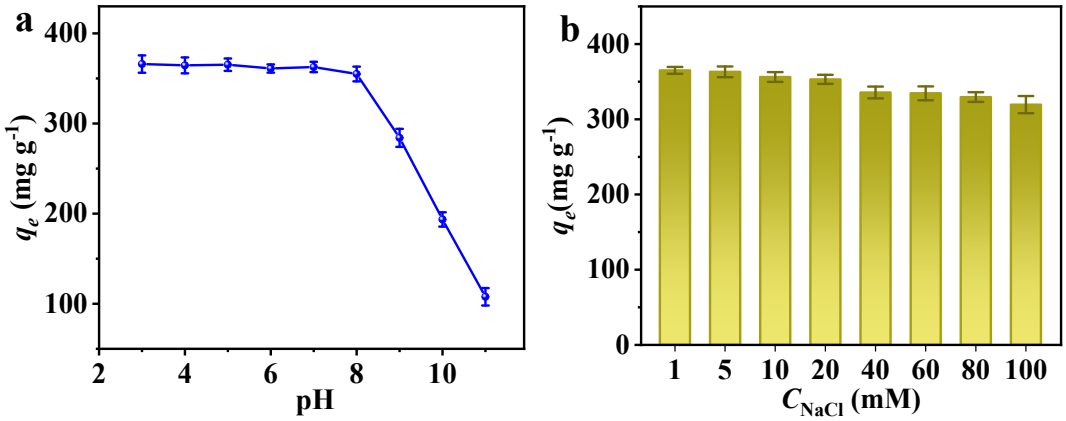

Fig. S14. Adsorption capacities of BPA (150 mg L^{-1}, 100 mL) on MWH-COPs (10.0 mg) under different pH values (3–11) (a) and ionic strength (1–100 mM) (b).

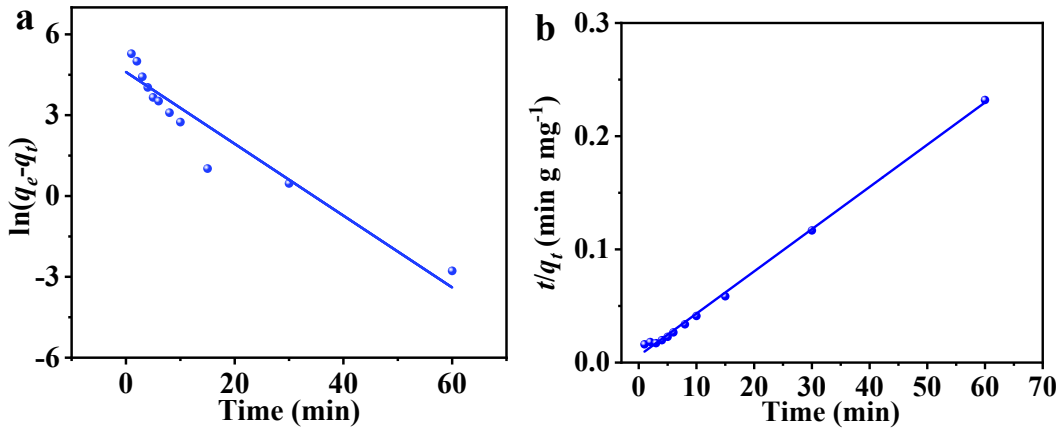

Fig. S15. Pseudo-first-order (a) and pseudo-second-order (b) models for BPA adsorption on MWH-COPs.

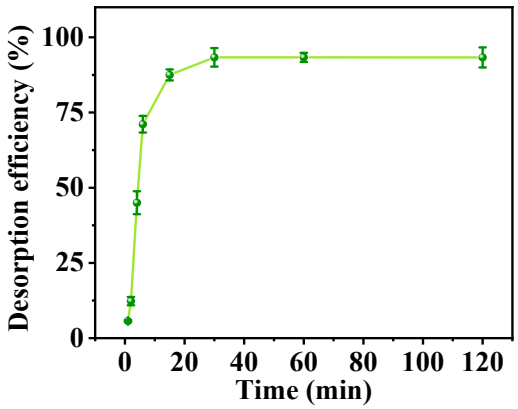

Fig. S16. Desorption efficiency by methanol/water (4/1, *v*/*v*) solution.

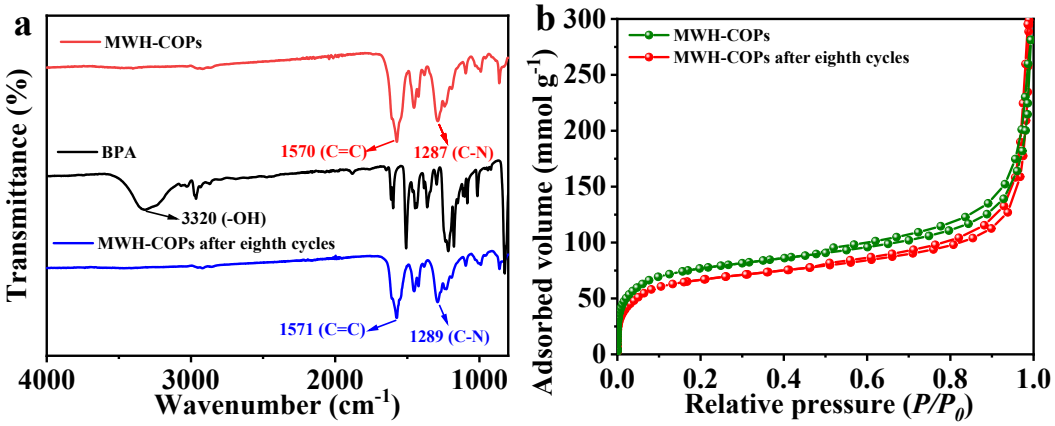

Fig. S17. FT-IR spectra (a) and N_2 sorption isotherms (b) of MWH-COPs before and after eight cycles.

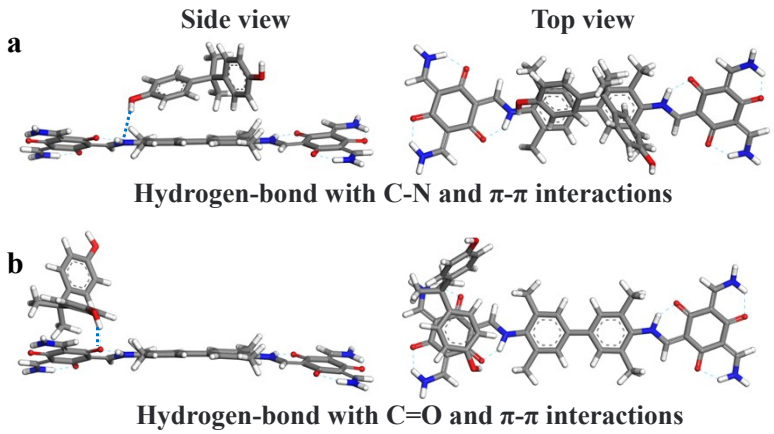

Fig. S18. Two equilibrium configurations (a and b) of BPA adsorption on MWH-COPs fragment.

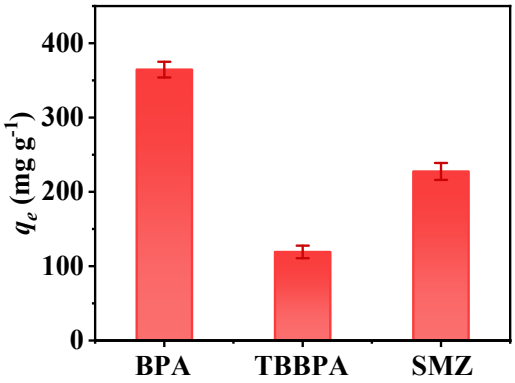

Fig. S19. Adsorption capacities on MWH-COPs with initial concentration at 150 mg L^{-1}.

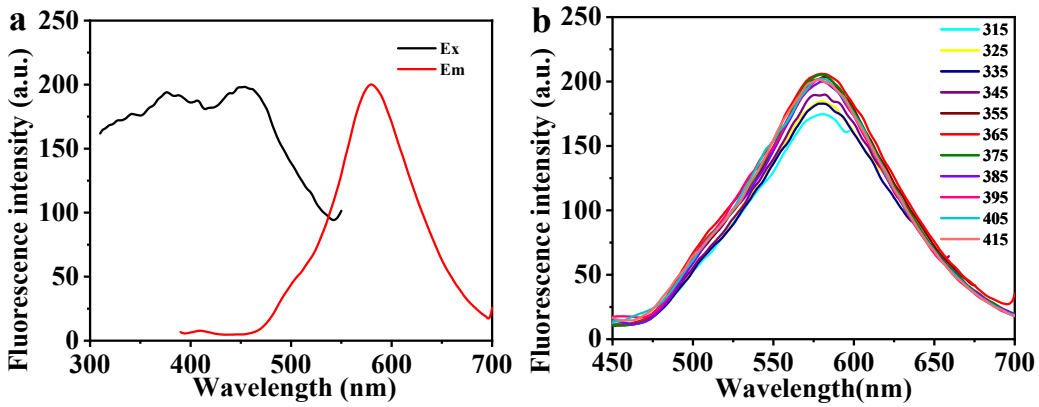

Fig. S20. (a) Fluorescence emission spectrum of MWH-COPs at 365 nm excitation,

and fluorescence excitation spectra of MWH-COPs at 578 nm emission; (b) Fluorescent spectra of MWH-COPs upon excitation at different wavelengths from 315 nm to 415 nm.

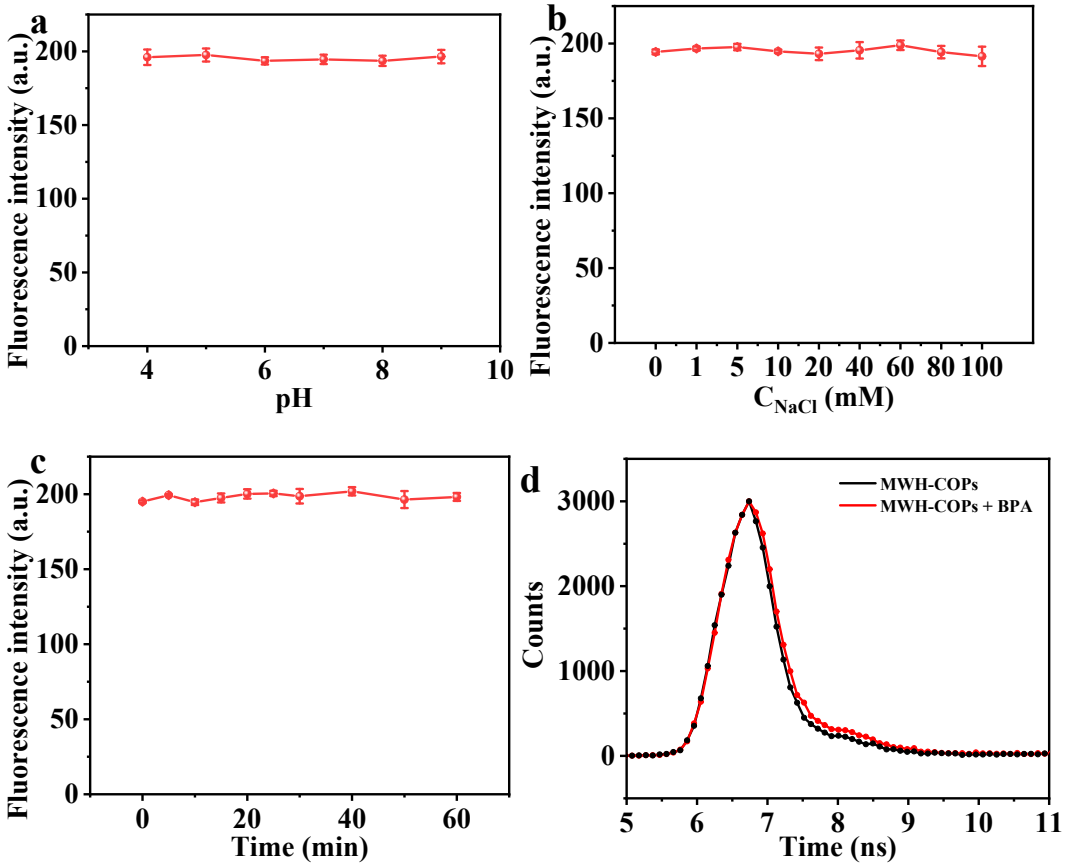

Fig. S21. Fluorescence intensity of MWH-COPs (0.02 mg mL^{-1}) in different pH (4–9), various NaCl concentrations (0–100 mM) (b), and at 365 nm irradiation for 60 min (c), Fluorescence decay curves of MWH-COPs before and after addition of 1.000 mg L^{-1} BPA (d).

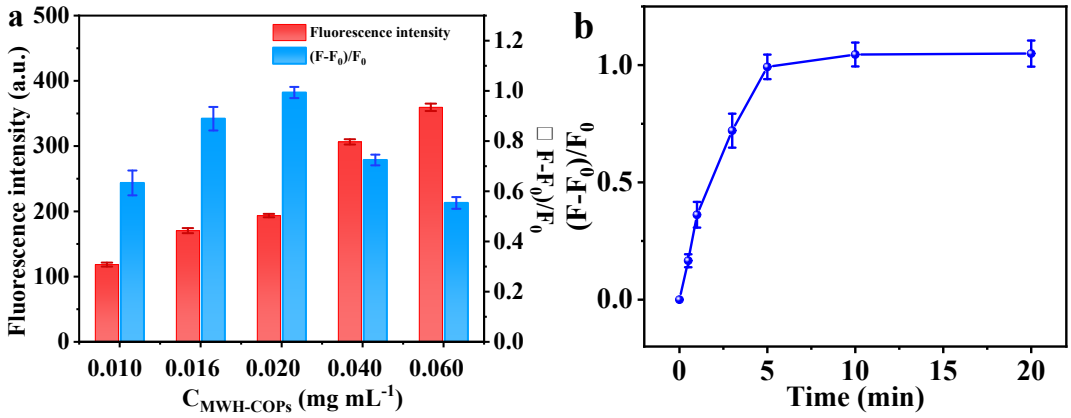

Fig. S22. (a) Effect of MWH-COPs concentration on fluorescence intensity and fluorescent enhancement efficiency with BPA (1.0 mg L^{-1}); (b) Effect of incubation time on fluorescent enhancement efficiency of MWH-COPs in the presence of BPA (1.0 mg L^{-1}).